Muon capture on the deuteron in chiral effective field theory

Jose Bonilla,[1,*] Bijaya Acharya,[2,†] and Lucas Platter[1,2,3,4,‡]

[1] *Department of Physics and Astronomy, University of Tennessee, Knoxville, TN 37996, USA*

[2] *Physics Division, Oak Ridge National Laboratory, Oak Ridge, TN 37831, USA*

[3] *Institut für Kernphysik, Technische Universität Darmstadt, 64289 Darmstadt, Germany*

[4] *ExtreMe Matter Institute EMMI, GSI Helmholtzzentrum für Schwerionenforschung GmbH, 64291 Darmstadt, Germany*

(Dated: March 15, 2023)

Abstract

We consider the capture of a muon on a deuteron. An uncertainty analysis of the dominant channels is important for a careful analysis of forthcoming experimental data. We quantify the theoretical uncertainties of chiral effective-field-theory predictions of the muon-deuteron capture rate from the relevant neutron-neutron partial wave channels in the final state. We study the dependence on the cutoff used to regularize the interactions, low-energy constants calibrated using different fitting data and strategies, and truncation of the effective-field-theory expansion of the currents. Combining these approaches gives as an estimate of $\Gamma_{\mu d}^{1/2} = 399.1 \pm 7.6 \pm 4.4$ s^{-1} for capture from the atomic doublet state, and $\Gamma_{\mu d}^{3/2} = 12.31 \pm 0.47 \pm 0.04$ s^{-1} for capture from the quartet state and the first and second uncertainties given here are due to the effective field theory truncation error and the uncertainty in the axial radius, respectively.

* jbonilla@vols.utk.edu

† bid@ornl.gov

‡ lplatter@utk.edu

I. INTRODUCTION

One of the main current priorities of nuclear theory is the description of nuclear electroweak processes. They give insights into the structure of complex nuclei, can be used to search for physics beyond the standard model, and are also important inputs to models of big bang nucleosynthesis and stellar evolution. Their calculation requires models of the nuclear interaction and electroweak currents that are consistent with each other. Chiral effective field theory provides a systematic approach to derive these consistently within one framework [1–3].

Effective field theories (EFTs) are systematic low-energy expansions that can be constructed when a system displays a separation of scales whose ratios can be used as the expansion parameters. Within chiral EFT, nucleons and pions are the degrees of freedom used to construct the nuclear Hamiltonian. The expansion parameter Q of chiral EFT is given by the ratio of the pion mass or a typical low momentum scale relevant for the problem at hand to Λ_b, the breakdown scale of the theory, which is expected to be comparable to the lightest degree of freedom not taken into account in the theory. The cost of this simplified EFT description of low-energy dynamics are additional parameters in the EFT, known as low-energy constants (LECs), that have to be determined by fitting to experiment or to calculations with the underlying theory. One important example of such parameters in chiral EFT are the two coupling constants c_D and c_E of the leading chiral three-body force whose values have to be determined by *matching* a theoretical calculation to experimental data. One of the two parameters is only related to short-distance three-nucleon physics, while the other is also related to the coupling of the electroweak current to the two-nucleon system. It should therefore be possible to obtain this coupling constant from an experimental measurement that involves only two nucleons. Muon capture on the deuteron, *i.e.* the process $\mu^- + d \to \nu_\mu + n + n$, is one such process that is experimentally accessible. The current operator thus calibrated can then be used to make predictions for other nuclear electroweak observables, *e.g.* the proton-proton fusion rate that serves as important input to astrophysical models but can not be measured at relevant energies.

Muon capture on nuclei has been a tool to study nuclear physics for a long time and the rate of muon capture on the deuteron has been experimentally measured several times in the past [4–7]. The precision of existing data, however, is not sufficient to guide theoretical

studies. An ongoing experiment at the Paul Scherrer Institute aims to measure this rate with 1.5% precision [8]. This will provide a strong constraint on the two-nucleon axial current operator which will be completely independent of the many-body dynamics that affect the extraction of c_D from $A \geq 3$ observables.

On the theoretical side, this process has been considered previously using different approaches, see for example Ref. [9] and references therein. The first chiral EFT calculation of muon capture into the neutron-neutron (nn) singlet S-wave was carried out by Ando *et al.* [10] in a hybrid formalism in which matrix elements are calculated with EFT currents and wave functions are obtained from phenomenological potentials. More recently, more complete calculations of this rate were carried out in Refs. [11, 12] (see also Ref. [13] for a review of EFT calculations of this process). It was pointed out in Ref. [14] (and confirmed in Ref. [15]) that previous works and other works on electroweak processes suffered from an error in the employed relation between the axial two-body current and the three-body force.

In Ref. [16], some of us considered previously the capture rate in chiral EFT with a focus on the ${}^1S_0$ neutron-neutron final state channel (with the correct relation between axial two-body current and three-body force). This channel gives the dominant contribution to the capture rate and is the only channel that is sensitive to the leading two-nucleon axial current in the chiral EFT expansion. In this work, we use the same chiral EFT interactions to consistently include higher partial-wave contributions, which is necessary to relate the ${}^1S_0$ capture rate to the experimental datum. We also note that a very recent calculation of muon capture into the deuteron doublet state with novel chiral EFT potentials that are minimally non-local [17] also aimed at quantifying the uncertainty of this process.

Here, we present a complete calculation of muon capture into doublet and quartet channel. We will take all relevant partial wave channels into account and quantify the uncertainty by using a large number of different chiral EFT interactions but also by estimating the EFT truncation error through an order-by-order calculation of this process.

This manuscript is ordered as follows. We discuss the electroweak current in chiral EFT in Section II and summarize the theoretical derivations needed to evaluate the muon capture rate in Section III. We then present our findings and put them in the context of previous literature in Section IV. We conclude with a brief summary and outlook in Section V.

II. ELECTROWEAK CURRENTS

Interactions between a system of particles and external sources are described by current operators that allow the transition from an initial state to a final state. In our case, these operators are the building blocks of the nuclear electroweak current J^μ that is written as a sum of vector and axial currents V^μ and A^μ, respectively

$$J^\mu = A^\mu_{1B} + V^\mu_{1B} + A^\mu_{2B} + V^\mu_{2B} \ , \tag{1}$$

where the subscripts $1B$ and $2B$ indicate whether we are considering a one-nucleon or two-nucleon current, respectively. Note that this combination of axial and vector currents along with the conserved vector current hypothesis imply that the vector part is related to the electromagnetic currents by isopin rotations. Expressions for these currents were previously derived in Refs. [18–21]. In this work, we use the currents derived with the method of unitary transformations by Kölling *et al.* [22] and Krebs *et al.* [23].

Consistent with the truncation of the nuclear potentials employed in the computation of the wavefunctions, we take into account current operators derived up to Q^0 (NNLO). Higher order terms are suppressed but the theory uncertainty from neglecting them are, as we will show below, comparable to the expected experimental uncertainties.

The current operators used in our work are displayed in Tbl. I, in which there are a variety of non-vanishing leading order (LO), next-to-leading order (NLO), and next-to-next-to-leading order (NNLO) contributions. The power-counting also includes relativistic corrections that are denoted by terms that have $1/m$ as subscript. Detailed expressions for the different terms for both axial and vector currents are given in Appendix A.

The first contribution to the total electroweak current appears at order Q^{-3} that includes a static one-body time-like vector operator Eq. (A6) and a one-body space-like axial operator Eq. (A2) which consists of the sum of the well known Gamow-Teller operator and a pion-pole contribution that is contained in the pseudoscalar form factor of this term. At order Q^{-1}, we encounter the one-body time-like axial operator Eq. (A1) which emerges from the time-dependence of unitary transformations and a leading relativistic $1/m$ correction. Moreover we have a space-like vector current contribution, shown in Eq. (A7), that includes the so-called convection current and the spin-magnetization terms. At this order and at Q^0, we include the two-body axial and vector current operators Eqs. (A3), (A4), (A5), and (A8).

J^μ	Q^{-3} (LO)	Q^{-1} (NLO)	Q^0 (NNLO)
A^0	-	$A^0_{1B:UT} + A^0_{1B:1/m} + A^0_{2B:1\pi}$	-
A^i	$A^i_{1B:static}$	-	$A^i_{2B:1\pi} + A^i_{2B:cont}$
V^0	$V^0_{1B:static}$	-	-
V^i	-	$V^i_{1B:static} + V^i_{1B:1/m} + V^i_{2B:1\pi}$	-

TABLE I. Ordering of the chiral electroweak currents as discussed in Refs. [22, 23]. Note that in this counting relativistic $1/m$ corrections are counted differently from the counting advocated by Park et al. [18]. Terms with a subscript *static* denote the contributions in which the external current couples directly to the nucleon, a subscript $1/m$ denotes relativistic corrections and the subscript 1π denotes contributions that include a pion loop.

We note that the space-like axial operators of Eqs. (A4) and (A5) feature LECs that also parametrize the pion-nucleon and three-nucleon forces. These are represented by c_i and c_D, respectively.

III. CALCULATION OF THE CAPTURE RATE

To obtain the capture rate, we first calculate the momentum-space matrix elements of the current operators discussed above, which are needed to evaluate the corresponding transition amplitude, defined as

$$T_{fi} = \frac{G_V}{\sqrt{2}} \psi_{\mu d}(0) \sum_{s_\mu, M_d} C^{f,f_z}_{1/2,s_\mu;1M_d}\; l^{\sigma-} \langle \Psi_f(\boldsymbol{p}) s_1 s_2 | \hat{J}_\sigma | \psi_d M_d \rangle \;\; , \tag{2}$$

where $G_V = 1.14939 \times 10^{-5}$ GeV^{-2} is the Fermi coupling constant taken from Ref.[12], $\psi_{\mu d}(0) = [\alpha_{\rm em} m_\mu m_d/(m_\mu + m_d)]^{3/2}/\pi^{1/2}$ is the ground state wavefunction of the muonic-deuterium atom at the origin and $\alpha_{\rm em}$ denotes the fine structure constant. The incoming state $|\psi_d M_d\rangle$ is the deuteron bound state with wave function ψ_d and total angular momentum projection M_d, and the outgoing state $|\Psi_f(\boldsymbol{p}) s_1 s_2\rangle$ is a neutron-neutron scattering state with wave function Ψ_f and with spin projections s_1 and s_2. Using a complete set of momentum states, we write the deuteron state as

$$|\psi_d, M_d\rangle = \sum_{l_d=0,2} \int dp p^2 \, |p(l_d 1); 1, M_d\rangle \otimes |0,0\rangle \, \psi_{l_d}(p) \;, \tag{3}$$

and we express the scattering state with relative momentum $\mathbf{p}$ by using the identity

$$\langle \Psi_f(\mathbf{p}) s_1 s_2| = \langle \mathbf{p} s_1 s_2| \left[\hat{1} + \hat{t}(E_{nn}) G_0(E_{nn})\right] \ , \tag{4}$$

here $\hat{t}$ denotes the solution of the Lippmann-Schwinger equation and G_0 is the free two-neutron Green's function, both evaluated at the two-neutron scattering energy $E_{nn} = \frac{p^2}{m_n}$. The leptonic tensor in Eq. (2) is given by

$$l^\sigma = \bar{u}(k', h)\gamma^\sigma(1 - \gamma_5)u(k, s_\mu) \ , \tag{5}$$

with lepton spinors $u(k, h)$. In addition to this, we employ a coupling between the muon-deuteron spin by introducing a Clebsch-Gordan coefficient $C^{f,f_z}_{1/2,s_\mu;1M_d}$ in Eq. (2) which allows to calculate the capture rates for the two hyperfine states $f = 1/2$ and $f = 3/2$.

Calculating the capture rate requires integration over the solid angle of $\mathbf{p}$. To relate the capture rate to the matrix elements with partial-wave projected final states, we express the transition amplitude of Eq. (2) in terms of spherical harmonics.

$$T_{fi} = \frac{G}{\sqrt{2}}\psi_{\mu d}(0) \sum_{s_\mu, M_d} C^{f,f_z}_{1/2,s_\mu;1,M_d} l^\sigma \sum_{\alpha, m_l, s_z} Y_l^{*m_l}(\hat{p}) C^{J,M_J}_{l,m_l;s,s_z} C^{s,s_z}_{1/2,s_1;1/2,s_2} \langle p\alpha| (\hat{1} + \hat{t}G_0) j_\sigma |\psi_d M_d\rangle \ . \tag{6}$$

Here, α denotes the channel with quantum numbers $\alpha \equiv \{(ls); JM_J\}$. In this work, we calculate the rate up to a $J \leq 2$ which includes the channels ${}^1S_0$, ${}^3P_0$, ${}^3P_1$, ${}^3P_2$, ${}^1D_2$, ${}^3F_2$ that make non-negligible contributions to the total muon capture rate. The integral over the solid angle of $\mathbf{p}$ then gives angle-averaged squared matrix elements which can be easily related to the total capture rate.

$$\Gamma^f_{\mu d} \propto \overline{|T_{fi}|^2} = \int d\hat{p} \frac{1}{2f+1} \sum_{f_z} \sum_{s_1, s_2} |T_{fi}|^2 \ . \tag{7}$$

To obtain the unpolarized rate, we then sum over the spin projections s_1 and s_2 of the outgoing nucleons, leading to

$$\overline{|T_{fi}|^2} \ = \ \frac{G_V^2}{2}|\psi_{\mu d}(0)|^2 \frac{1}{2f+1} \sum_{f_z} \sum_{\alpha} \left| \sum_{s_\mu, M_d} C^{f,f_z}_{1/2,s_\mu;1,M_d} \ l^\sigma \langle p\alpha| (\hat{1} + \hat{t}G_0) \hat{J}_\sigma |\psi_d M_d\rangle \right|^2 \ . \tag{8}$$

Finally, the momentum distribution of the capture rate for any channel can be calculated by carrying out the phase space integral over the momentum of the outgoing neutrino, which yields

$$\frac{d\Gamma^f_{\mu d}}{dp} = \frac{2}{\pi} E_\nu^2 p^2 \frac{m_n}{E_\nu + 2m_n} \overline{|T_{fi}|^2} \ . \tag{9}$$

$g_A = 1.2754$	Capture Rate 1B $\Gamma^f_{\mu d}(s^{-1})$					
	$f = 1/2$			$f = 3/2$		
NNLOsim	$^1S_0$	$J \leq 1$	$J \leq 2$	$^1S_0$	$J \leq 1$	$J \leq 2$
$\Lambda = 450$ MeV	248.73	305.97	386.27	6.64	7.66	11.23
$\Lambda = 475$ MeV	248.14	305.95	386.25	6.62	7.66	11.26
$\Lambda = 500$ MeV	247.61	305.80	386.12	6.61	7.66	11.29
$\Lambda = 525$ MeV	247.14	305.57	385.90	6.60	7.66	11.31
$\Lambda = 550$ MeV	246.73	305.34	385.68	6.59	7.65	11.32
$\Lambda = 575$ MeV	246.37	305.10	385.47	6.58	7.65	11.33
$\Lambda = 600$ MeV	246.07	304.90	385.28	6.57	7.64	11.33
A. Elmeshneb [24]	240.5	303.3	383.4	6.38	7.73	11.31

TABLE II. Results for the muon capture rate for the doublet ($f = 1/2$) and quartet ($f = 3/2$) channel obtained with the NNLOsim [25] interactions and NNLO one-body currents only. The different rows give the results obtained with different momentum cutoff Λ. Each given value is the average over the 6 NNLOsim interactions with different T^{lab}_{max} truncations at this cutoff. Different columnns give the result for the rate with channels included up to $J = 0, 1$, or 2. The last row shows the corresponding results given in Ref. [24] for comparison.

The energy of the neutrino in Eq. (9) is given by $E_\nu = \frac{1}{2(m_\mu + m_d)}\left[(m_\mu + m_d)^2 - 4(m_n^2 + p^2)\right]$, where m_μ, m_d, and m_n are the masses of the muon, deuteron, and the neutron respectively. The total capture rate $\Gamma^f_{\mu d}$ can be calculated by integrating Eq. (9) over the relative momentum p from 0 to $p_{max} = \left[\frac{(m_\mu + m_d)^2}{4} - m_n^2\right]^{1/2}$. We use 120 p points to achieve convergency in our results.

IV. RESULTS

For the calculation of the μd-capture rate, we first use a family of 42 interactions truncated at NNLO. The NN and NNN LECs in these interactions have been fitted in Ref. [25] at seven different values of the regulator cutoff Λ at 25 MeV intervals in the range from 450 to 600 MeV simultaneously to the pion-nucleon data, the energies and charge radii of ^{2,3}H and ^{3}He, the one-body quadrupole moment of ^{2}H, the comparative β-decay half life of ^{3}H as well as six different pools of NN scattering data with different truncations in the NN scattering energy,

Capture Rate for Doublet State 1B+2B $\Gamma_{\mu d}^{1/2}(s^{-1})$							
NNLOsim	$^1S_0$	$^3P_0$	$^3P_1$	$^3P_2$	$^1D_2$	$^3F_2$	Total
$\Lambda = 450$ MeV	255.04	15.27	45.55	71.88	7.75	0.97	396.46
$\Lambda = 500$ MeV	254.44	16.02	45.72	71.93	7.75	0.98	396.84
$\Lambda = 550$ MeV	253.48	16.32	45.84	72.00	7.75	0.98	396.37
$\Lambda = 600$ MeV	252.09	16.47	45.89	72.06	7.76	0.98	395.25
$\text{NNLO}_{\text{RS450}}$ ($\Lambda = 450$ MeV)	$^1S_0$	$^3P_0$	$^3P_1$	$^3P_2$	$^1D_2$	$^3F_2$	Total
LO	189.36	13.60	30.23	58.98	5.88	0.70	298.75
NLO	250.92	19.28	47.08	72.05	7.91	1.00	398.24
NNLO	254.39	19.23	47.07	72.31	7.89	1.01	401.90
Theoretical Results:							
S. Ando *et al.* [10]	386±4						
L.E. Marcucci *et al.* [11]	399±3						
A. Elmeshneb [24]	401						
Experimental Results:							
I.-T. Wang *et al.* [4]	365±96						
A. Bertin *et al.* [5]	445±60						
M. Martino [6]	470±29						
M. Cargnelli *et al.* [7]	409±40						

TABLE III. Results for the muon capture rate for the doublet ($f = 1/2$) channel in s^{-1}. Different columns give the results for the different partial wave channels included. The labels NNLOsim and NNLO_{RS} indicate the nucleon-nucleon interaction at order Q^3 used to calculate deuteron and nn wave functions.

T_{lab}. These interactions, which we denote by NNLOsim, have been refitted to account for an error in the equation that relates c_D to the axial two-body contact current and then used to calculate muon capture into the $^1\text{S}_0$ nn-channel [16]. This error was found by the authors of Ref. [14] and a detailed discussion of this correction was later published in Ref. [15] (see also Ref. [16]). Here, we have calculated the rate for muon capture for the other five additional partial wave channels that give a sizeable contribution to the rate and are therefore important for comparison with experiment. While the NNLOsim interactions capture uncertainties from cutoff variation, sensitivity to the input data sets, and fitting errors that account for

Capture Rate for Quartet State 1B+2B $\Gamma^{3/2}_{\mu d}(s^{-1})$							
NNLOsim	$^1S_0$	$^3P_0$	$^3P_1$	$^3P_2$	$^1D_2$	$^3F_2$	Total
$\Lambda = 450$ MeV	6.72	0.54	0.50	1.53	2.58	0.34	12.21
$\Lambda = 500$ MeV	6.71	0.57	0.51	1.54	2.68	0.34	12.35
$\Lambda = 550$ MeV	6.69	0.58	0.51	1.56	2.75	0.35	12.44
$\Lambda = 600$ MeV	6.68	0.59	0.51	1.56	2.79	0.35	12.48
$\text{NNLO}_{\text{RS450}}$ ($\Lambda = 450$ MeV)	$^1S_0$	$^3P_0$	$^3P_1$	$^3P_2$	$^1D_2$	$^3F_2$	Total
LO	2.77	0.40	0.21	0.64	1.29	0.13	5.44
NLO	6.63	0.75	0.52	1.48	1.84	0.33	11.55
NNLO	6.72	0.75	0.51	1.53	2.39	0.34	12.24
Theoretical Results:							
A. Elmeshneb [24]	12.7						

TABLE IV. Rate results for muon capture on the deuteron for hyperfine state $f = 3/2$ (quartet). Results are calculated using partial wave decomposition approach and are displayed in each corresponding channel upto a $J \leq 2$. The labels NNLOsim and NNLO_{RS} indicate the nucleon-nucleon interaction at order Q^3 used to calculate deuteron and nn wave functions.

correlations among the LECs, it is also instructive to fix the pion-nucleon LECs to the precise values obtained in Refs. [26, 27] using Roy-Steiner analysis. To this end, we use the LO, NLO and NNLO interactions of Ref. [28], which we name LO_{RS450}, $\text{NLO}_{\text{RS450}}$, and $\text{NNLO}_{\text{RS450}}$. These interactions have been fit to the Granada database [29–31] as well as the nn effective range parameters [32] with the pion-nucleon constants appearing at NNLO fixed at the central values of the NLO [33] pion-nucleon coupling constants of Ref. [27]. The various orders of the RS450 interactions also allow us to compare the uncertainty from the truncation error in the potential to the NNLOsim uncertainties, which is an important check of self-consistency of chiral EFT [34].

We show the results for the capture rates (capture from doublet and quartet channel, and the channels included, truncated at different total nuclear angular momentum J_{max}) obtained with differently regulated NNLOsim and one-body currents only in Tbl. II. Here, each entry is the average over the set of NNLOsim interactions with different T_{lab} truncations at a given regulator Λ. The last row shows the corresponding results given in Ref. [24] that we obtained

with wave functions from chiral EFT potentials, the standard one-body operators, and phenomenological two-body currents. In Tbl. III, we show the results for the doublet capture rate obtained with NNLOsim potentials and one- and two-body currents, the corresponding results obtained with the RS450 interactions at LO, NLO and NNLO, the experimental results given in Refs. [4–7], and the theoretical results obtained in Refs. [10, 12, 24]. The different columns give now the contribution for each individual channel included with the last one giving the total capture rate.

To demonstrate the impact of the inclusion of final state interactions, we show in Figs. 2 and 3, the differential capture rate with (bottom panel) and without final state interactions (top panel) as a function of the magnitude of the relative momentum p between the outgoing neutrons for doublet and quartet channel, respectively. The differently colored solid lines denote the contributions from the individual partial wave channels of the nn state. The dashed line denotes the total differential capture rate. The widths of these lines is generated through the calculation of the partial differential capture rate with the different 42 different NNLOsim interactions. It can clearly be seen that for both rates (doublet and quartet), capture into the $^1S_0$ channel gives the largest contribution but also that a number of different channels give sizeable contributions. The total differential capture rates for doublet and quartet channel are in qualitative agreement with the results shown in Ref. [24] that were obtained with chiral wave functions and phenomenological two-body currents.

In the top (bottom) panel of Fig. 1, we show the full rate $\Gamma_{\mu d}^{1/2}$ for capture from the doublet (quartet) channel for the 42 different chiral interactions. We obtain the central values of our rates by averaging the 42 results in each channel. The spread between the smallest and largest rate and the corresponding central value give us an estimate for the rate and its uncertainty. This is shown as the first error in Eq. (10) below. We also propagate the recently determined uncertainty in the axial radius $r_A^2 = 0.46 \pm 0.16$ fm^2 [35] by calculating the rates at the upper and lower range of this uncertainty estimate. This is shown as the second (symmetrical) error in Eq. (10) below. For the doublet and quartet channel rate, we obtain in this way

$$\begin{aligned} \left[\Gamma_{\mu d}^{1/2}\right]_{\rm sim} &= (396.33^{+0.94}_{-1.85} \pm 4.4)\text{s}^{-1} \ , \\ \left[\Gamma_{\mu d}^{3/2}\right]_{\rm sim} &= (12.38^{+0.34}_{-0.25} \pm 0.04)\text{s}^{-1} \ . \end{aligned} \tag{10}$$

An even more reliable way to determine the uncertainty of an EFT calculation is to study

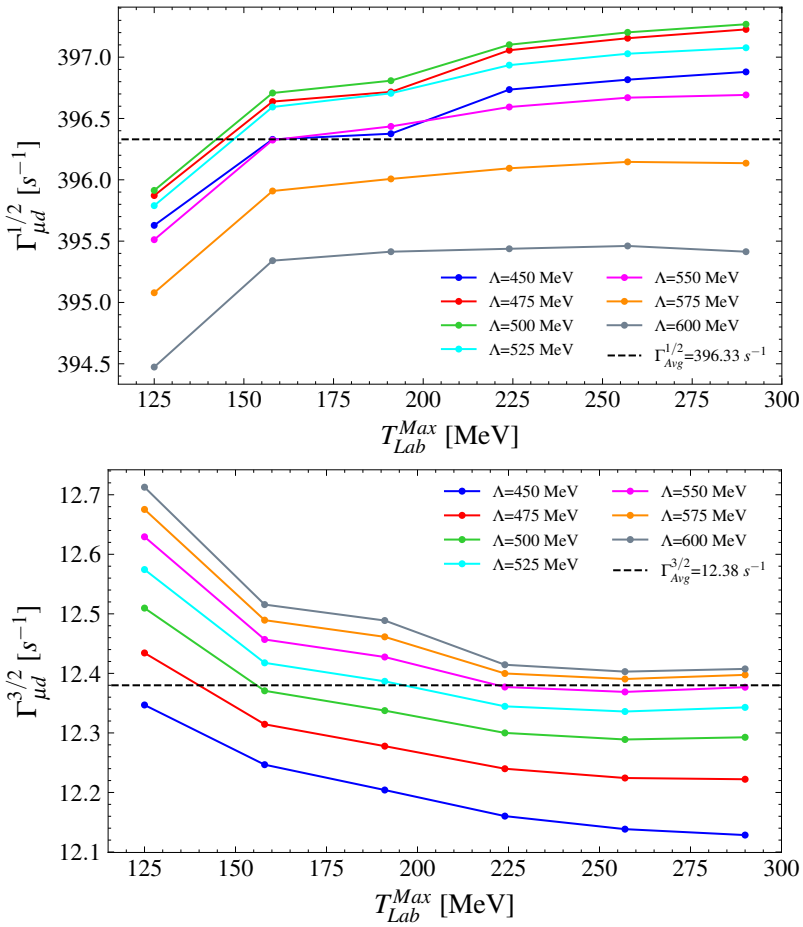

FIG. 1. Top panel: Total muon capture rate on the deuteron evaluated for the doublet channel. Bottom panel: Total muon capture rate on the deuteron evaluated for the quartet channel. Results includes contributions for the nn-channels up to $J \leq 2$. Each point represents the result obtained with one of the 42 NNLOsim potentials at order Q^3 from Ref. [25]. Results with the same cutoffs are connected by a line to guide the eye.

the order-by-order convergence pattern of an observable. Here, we will follow the method discussed in Ref. [36] by writing the capture rate for either doublet or quartet channel as

$$\Gamma_{\mu d} = \Gamma^{\rm LO}_{\mu d} \sum_{n=0}^{3} c_n \left(\frac{p}{\Lambda_b}\right)^n , \tag{11}$$

where $\Gamma^{\rm LO}_{\mu d}$ denotes the leading order result for the muon capture rate (in either doublet or quartet channel), p denotes the inherent momentum scale of the problem, and Λ_b is the breakdown scale. An estimate of the truncation is then obtained by calculating $(p/\Lambda_b)^4 \max(|c_0|, |c_2|, |c_3|)$. Using the RS450 results of Tbl. III and Tbl. IV to obtain the

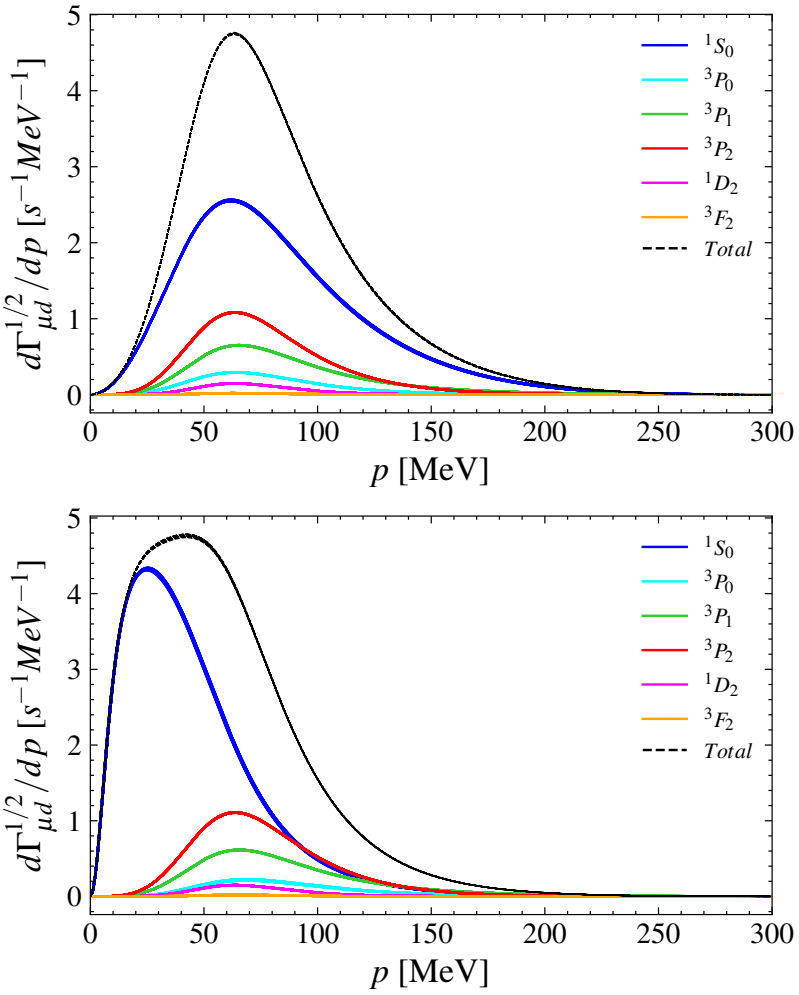

FIG. 2. Top panel: Differential capture rate results for the doublet channel $f = 1/2$ calculated without final state interactions. Bottom panel: Differential capture rate results for the doublet channel $f = 1/2$ calculated with final state interactions. The solid lines give the results for different nn partial wave channels. The dashed solid lines give the total differential capture rate.

c_i's, the pion mass for the momentum scale p and $\Lambda_b = 500$ MeV, we obtain an uncertainty of 7.6 s^{-1} for the total doublet channel capture rate and 0.47 s^{-1} for the total quartet capture rate.

Using these results at face value we obtain for the μd-capture from this approach gives

$$\left[\Gamma_{\mu d}^{1/2}\right]_{\rm RS450} = (401.90 \pm 7.6 \pm 4.4)\ s^{-1}\ ,$$
$$\left[\Gamma_{\mu d}^{3/2}\right]_{\rm RS450} = (12.24 \pm 0.47 \pm 0.04)\ s^{-1}\ , \qquad (12)$$

where the first uncertainty quoted above is the estimate for the EFT truncation error and

the second is the uncertainty resulting from the quoted uncertainty in the axial radius. The uncertainty for the doublet prediction is in good agreement with the uncertainty obtained using the same method for capture into $^1S_0$ channel in Ref. [16] but also with the spread in the final results between NNLOsim and $\text{NNLO}_{\text{RS450}}$ interactions.

To obtain a final recommendation for the μd-capture rates in doublet an quartet channel we take the average of the values given in Eqs. (10),(12) and use the uncertainties of Eq. (12)

$$\Gamma_{\mu d}^{1/2} = (399.1 \pm 7.6 \pm 4.4)\ \text{s}^{-1}\ , \tag{13}$$

$$\Gamma_{\mu d}^{3/2} = (12.31 \pm 0.47 \pm 0.04)\ \text{s}^{-1}\ . \tag{14}$$

Within the quoted truncation error, our results agree with the previously published theoretical results in Refs. [11, 24] but disagrees slightly with the result given in Ref.[10]. The results for capture into the doublet $^1S_0$ channel alone also agree well with the recent calculation presented in Ref. [17]. Our result for doublet capture also compare favorably with the experimental results [4–7]., however their large uncertainties limit our abilities to conclusions about the quality of the employed currents.

V. CONCLUSION

In this work, we have calculated the total μd-capture from doublet and quartet channel using chiral EFT potentials at NNLO and consistent NNLO currents [22, 23]. For the total rates, we find after combining the results from different interactions $\Gamma_{\mu d}^{1/2} = 399.1 \pm 7.6 \pm 4.4$ s^{-1} for capture from the doublet channel, and $\Gamma_{\mu d}^{3/2} = 12.31 \pm 0.47 \pm 0.04$ s^{-1} for capture from the quartet channel. The first uncertainty quoted above arises from the order by order convergence pattern of the capture rates, the second uncertainty propagates from the quoted uncertainty in the axial radius. The recently determined large uncertainty of the axial radius [35] remains therefore a pressing problem for the analysis of this problem as it prevents a reliable connection of the experimental results with the nuclear Hamiltonian. However, the large uncertainty in the doublet capture rate due to the intrinsic error of chiral EFT also highlights that an experimental result for the capture rate can provide important information on the nuclear Hamiltonian.

The results for the differential capture rate and the total capture rate are in good agreement with previously published theoretical predictions [10–12, 24] apart from a small dis-

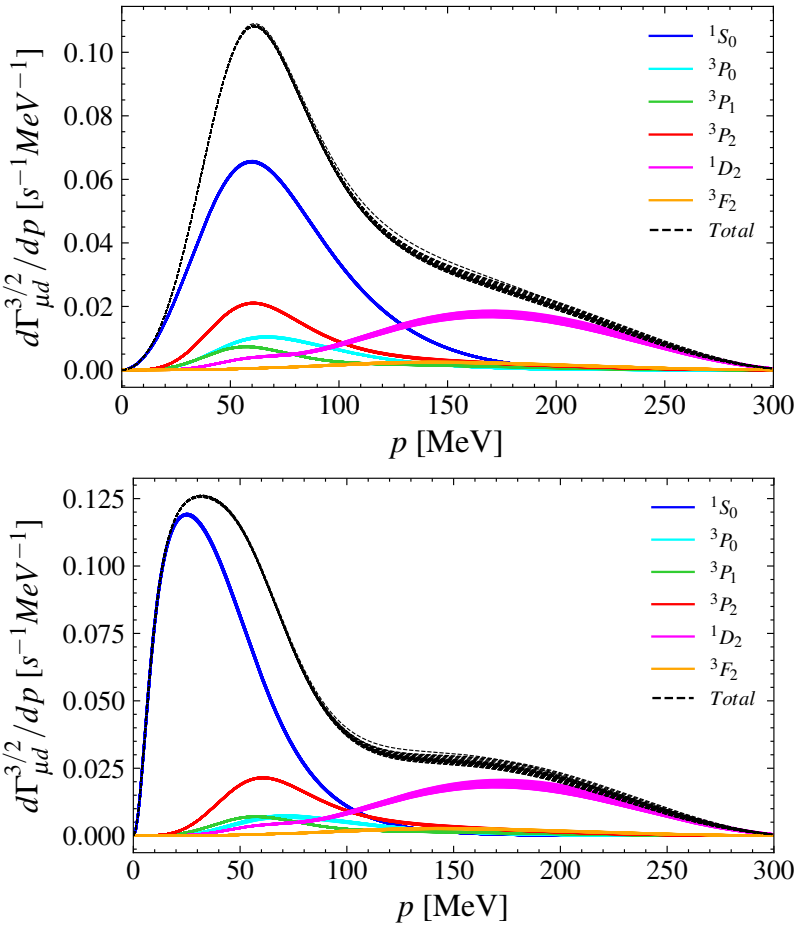

FIG. 3. Top panel: Differential capture rate results for the quartet channel $f = 3/2$ calculated without final state interactions. Bottom panel: Differential capture rate results for the quartet channel $f = 3/2$ calculated with final state interactions. The solid lines give the results for different nn partial wave channels. The dashed solid lines give the total differential capture rate.

crepancy with the $^1D_2$ doublet capture rate quoted in [11]. To the best of our knowledge, this work represents the first EFT calculation of the capture rate from the quartet channel.

This and previous works demonstrate that muon capture on light nuclei is a valuable tool to study the nuclear Hamiltonian. It is impacted by superpositions of current matrix elements in a non-trivial way and depends also strongly on an accurate descriptions of nuclear bound and scattering properties. An ambitious program that focuses on the reduction of experimental uncertainties and combined with capture rate calculations for different processes might have the potential of constraining the additional short-range counterterms that appear in the axial and vector current at order Q [22, 23]. Furthermore, a full calculation of

radiative corrections such as the Wγ box contribution seams feasible and therefore desirable. In particular, to assess the importance of those contributions that can not be expressed as one-nucleon radiative corrections and their dependence on nuclear structure effects [37].

ACKNOWLEDGMENTS

We acknowledge useful discussions with Evgeny Epelbaum, Jacek Golak and Andreas Ekström. This work has been supported by the National Science Foundation under Grant Nos. PHY-1555030 and PHY-2111426 and by the Office of Nuclear Physics, U.S. Department of Energy under Contract No. DE-AC05-00OR22725. BA is supported by the Neutrino Theory Network Fellowship Program (Grant No. DE-AC02-07CH11359). This work used the Bridges-2 computing resource at the Pittsburgh Supercomputing Center through allocation PHY220101 from the Advanced Cyberinfrastructure Coordination Ecosystem: Services & Support (ACCESS) program, which is supported by National Science Foundation grants #2138259, #2138286, #2138307, #2137603, and #2138296.

Appendix A: Electroweak Currents

1. Axial currents

The zero-component of the one-body axial current contains contributions from the axial and pseudoscalar form factor

$$A^0_{1B} = \left[-\frac{G_A(-\mathbf{q}^2)}{m} \boldsymbol{q}_1 \cdot \boldsymbol{\sigma}_1 + \frac{G_P(-\mathbf{q}^2)}{4m^2} q_0 \boldsymbol{q} \cdot \boldsymbol{\sigma}_1 \right] \tau_{-,1} \ + \ (1 \to 2) \ , \tag{A1}$$

where we use $m = 938.9$ MeV and expressions for G_A and G_P will be given below. The vector components of the axial current are

$$\mathbf{A}_{1B} = \left[-G_A(-\mathbf{q}^2)\boldsymbol{\sigma}_1 + \frac{G_P(-\mathbf{q}^2)}{4m^2} \boldsymbol{q} (\boldsymbol{q} \cdot \boldsymbol{\sigma}_1) \right] \tau_{-,1} \ + \ (1 \to 2) \ , \tag{A2}$$

where $\boldsymbol{q} = \boldsymbol{p}'_i - \boldsymbol{p}_i$, $\boldsymbol{q}_i = (\boldsymbol{p}'_i + \boldsymbol{p}_i)/2$, and $q_0 = (\boldsymbol{p}'^2_i - \boldsymbol{p}^2_i)/2m$.

The axial two-body currents used in this work have the form

$$A^0_{2B:1\pi} = -i \frac{g_A}{4F_\pi^2} \frac{\boldsymbol{k}_1 \cdot \boldsymbol{\sigma}_1}{k_1^2 + m_\pi^2} [\boldsymbol{\tau}_1 \times \boldsymbol{\tau}_2]_- \ + \ (1 \leftrightarrow 2) \ , \tag{A3}$$

where we use throughout this work $g_A = 1.2754$ [38], $F_\pi = 92.4$ MeV [25], and $m_\pi = 138.039$ MeV. and

$$\mathbf{A}_{2B:1\pi} = \frac{g_A}{2F_\pi^2}\frac{\boldsymbol{\sigma}_1\cdot\boldsymbol{k}_1}{k_1^2+m_\pi^2}\Bigg\{\tau_{-,1}\left[-8c_1m_\pi^2\frac{\boldsymbol{q}}{q^2+m_\pi^2}+4c_3\left(\boldsymbol{k}_1-\frac{\boldsymbol{q}\,\boldsymbol{q}\cdot\boldsymbol{k}_1}{q^2+m_\pi^2}\right)\right] + c_4[\boldsymbol{\tau}_1\times\boldsymbol{\tau}_2]_-\left(\boldsymbol{k}_1\times\boldsymbol{\sigma}_2-\frac{\boldsymbol{q}\,\boldsymbol{q}\cdot\boldsymbol{k}_1\times\boldsymbol{\sigma}_2}{q^2+m_\pi^2}\right)-\frac{\kappa_v}{4m}[\boldsymbol{\tau}_1\times\boldsymbol{\tau}_2]_-\boldsymbol{q}\times\boldsymbol{\sigma}_2\Bigg\} \;+\; (1\leftrightarrow 2) \quad \text{(A4)}$$

$$\mathbf{A}_{2B:cont} = -\frac{c_D}{2F_\pi^2\Lambda_\chi}\left[\boldsymbol{\sigma}_1-\frac{\boldsymbol{q}(\boldsymbol{\sigma}_1\cdot\boldsymbol{q})}{q^2+{m_\pi}^2}\right]\tau_{-,1} \;+\; (1\leftrightarrow 2)\;, \quad \text{(A5)}$$

where $\boldsymbol{k}_i = \boldsymbol{p}_i' - \boldsymbol{p}_i$, $q = |\boldsymbol{q}|$, κ_v is the isovector anomalous magnetic moment of the nucleon, $\Lambda_\chi = 700$ MeV is the chiral symmetry breaking scale of the order of the ρ meson mass.

2. Vector currents

The zero-component of the one-body vector current takes the standard form

$$V_{1B}^0 = G_E(t)\;\tau_{-,1} \;+\; (1\to 2)\;. \quad \text{(A6)}$$

The spatial components of the one-body vector current operator receive the standard contributions from the electric and magnetic couplings encoded in the electric and magnetic form factors G_E and G_M, respectively

$$\mathbf{V}_{1B} = \left[\frac{G_E(t)}{m}\boldsymbol{q}_1 - i\frac{G_M(t)}{2m}\big(\boldsymbol{q}\times\boldsymbol{\sigma}_1\big)\right]\tau_{-,1} \;+\; (1\to 2)\;, \quad \text{(A7)}$$

where we defined the four-momentum transfer $t = q_0^2 - \mathbf{q}^2 = m_\mu(m_\mu - 2E_\nu)$, with $\mathbf{q} = E_\nu\,\hat{z}$. The two-body current that enters at NLO is

$$\mathbf{V}_{2B:1\pi} = i\frac{g_A^2}{4F_\pi^2}\frac{\boldsymbol{\sigma}_2\cdot\boldsymbol{k}_2}{k_2^2+{m_\pi}^2}\left[\boldsymbol{k}_1\frac{\boldsymbol{\sigma}_1\cdot\boldsymbol{k}_1}{k_1^2+{m_\pi}^2}-\boldsymbol{\sigma}_1\right][\boldsymbol{\tau}_1\times\boldsymbol{\tau}_2]_- \;+\; (1\leftrightarrow 2)\;. \quad \text{(A8)}$$

3. Axial-Vector Form Factors

a. Axial Form Factors

We parametrize the axial form factor as in Ref. [23]

$$G_A(-\mathbf{q}^2) = g_A\left(1-\frac{\langle r_A^2\rangle}{6}\mathbf{q}^2\right) \quad \text{(A9)}$$

with the axial radius squared $\langle r_A^2 \rangle = 0.46(16)$ fm^2. The pseudoscalar form factor is

$$G_P(-\mathbf{q}^2) = \frac{4m^2}{\mathbf{q}^2 + m_\pi^2} g_A \ , \tag{A10}$$

where we emphasize that we found no difference in using this parametrization versus using the form employed in Ref. [12] that replaces the factor of g_A with the axial form factor.

b. Vector Form Factors

In the currents defined above we employ the isovector combination of the electric (magnetic) proton and neutron form factors G_E^p and G_E^n (G_M^p and G_M^n) [39], respectively

$$G_E = G_E^p - G_E^n \quad and \quad G_M = G_M^p - G_M^n \tag{A11}$$

The electric form factors are parametrized with dipole factors G_D

$$G_E^p(t) = G_D(t) \quad and \quad G_E^n(t) = \mu_n \frac{t}{4m^2} \frac{G_D(t)}{1 - t/m^2} \ , \tag{A12}$$

with the magnetic moments of proton and neutron $\mu_p = 2.793$ $\mu_n = -1.913$ in units of nuclear magnetons. The dipole form factor is defined as

$$G_D(t) = \frac{1}{(1 - t/\Lambda_V^2)^2} \ , \tag{A13}$$

where $\Lambda_V = 0.833$ GeV. The magnetic form factors of proton and neutron are written as

$$G_M^p(t) = \mu_p G_D(t) \quad and \quad G_M^n(t) = \mu_n G_D(t) \ . \tag{A14}$$

[1] P. F. Bedaque and U. van Kolck, Ann. Rev. Nucl. Part. Sci. **52**, 339 (2002), arXiv:nucl-th/0203055.

[2] E. Epelbaum, H. W. Hammer, and U.-G. Meissner, Rev. Mod. Phys. **81**, 1773 (2009), arXiv:0811.1338 [nucl-th].

[3] H.-W. Hammer, A. Nogga, and A. Schwenk, Rev. Mod. Phys. **85**, 197 (2013), arXiv:1210.4273 [nucl-th].

[4] I.-T. Wang, E. W. Anderson, E. J. Bleser, L. M. Lederman, S. L. Meyer, J. L. Rosen, and J. E. Rothberg, Phys. Rev. **139**, B1528 (1965).

[5] A. Bertin, A. Vitale, A. Placci, and E. Zavattini, Phys. Rev. D **8**, 3774 (1973).

[6] J. Martino, Nucl. Phys. A **453**, 591 (1986).

[7] M. Cargnelli, W. H. Breunlich, H. Fuhrmann, P. Kammel, J. Marton, P. Pawlek, J. Werner, J. Zmeskal, W. Bertl, and C. Petitjean, in *23rd Yamada Conference: Nuclear Weak Processes and Nuclear Structure* (1989) pp. 115–120.

[8] P. Kammel (MuSun), SciPost Phys. Proc. **5**, 018 (2021).

[9] D. F. Measday, Phys. Rept. **354**, 243 (2001).

[10] S. Ando, T. S. Park, K. Kubodera, and F. Myhrer, Phys. Lett. **B533**, 25 (2002), arXiv:nucl-th/0109053 [nucl-th].

[11] L. E. Marcucci, A. Kievsky, S. Rosati, R. Schiavilla, and M. Viviani, Phys. Rev. Lett. **108**, 052502 (2012), arXiv:1109.5563 [nucl-th].

[12] L. E. Marcucci, M. Piarulli, M. Viviani, L. Girlanda, A. Kievsky, S. Rosati, and R. Schiavilla, Phys. Rev. **C83**, 014002 (2011), arXiv:1008.1172 [nucl-th].

[13] L. E. Marcucci, Int. J. Mod. Phys. A **27**, 1230006 (2012), arXiv:1112.0113 [nucl-th].

[14] L. E. Marcucci, A. Kievsky, S. Rosati, R. Schiavilla, and M. Viviani, Phys. Rev. Lett. **121**, 049901 (2018).

[15] D. Gazit, S. Quaglioni, and P. Navrátil, Phys. Rev. Lett. **122**, 029901 (2019).

[16] B. Acharya, A. Ekström, and L. Platter, Phys. Rev. C **98**, 065506 (2018).

[17] L. Ceccarelli, A. Gnech, L. E. Marcucci, M. Piarulli, and M. Viviani, Front. Phys. **10**, 1049919 (2023), arXiv:2209.09762 [nucl-th].

[18] T.-S. Park, D.-P. Min, and M. Rho, Nucl. Phys. **A596**, 515 (1996), arXiv:nucl-th/9505017 [nucl-th].

[19] T.-S. Park, K. Kubodera, D.-P. Min, and M. Rho, Astrophys. J. **507**, 443 (1998), arXiv:astro-ph/9804144 [astro-ph].

[20] T. S. Park *et al.*, Phys. Rev. **C67**, 055206 (2003), arXiv:nucl-th/0208055.

[21] Y.-H. Song, R. Lazauskas, and T.-S. Park, Phys. Rev. **C79**, 064002 (2009), arXiv:0812.3834 [nucl-th].

[22] S. Kolling, E. Epelbaum, H. Krebs, and U. G. Meissner, Phys. Rev. C **84**, 054008 (2011), arXiv:1107.0602 [nucl-th].

[23] H. Krebs, E. Epelbaum, and U. G. Meißner, Annals Phys. **378**, 317 (2017), arXiv:1610.03569 [nucl-th].

[24] A. Elmeshneb, *Muon capture on the deuteron and 3He*, Ph.D. thesis, Jagiellonian U. (main) (2015).

[25] B. D. Carlsson, A. Ekström, C. Forssén, D. F. Strömberg, G. R. Jansen, O. Lilja, M. Lindby, B. A. Mattsson, and K. A. Wendt, Phys. Rev. **X6**, 011019 (2016), arXiv:1506.02466 [nucl-th].

[26] M. Hoferichter, J. Ruiz de Elvira, B. Kubis, and U.-G. Meißner, Phys. Rept. **625**, 1 (2016), arXiv:1510.06039 [hep-ph].

[27] D. Siemens, J. R. de Elvira, E. Epelbaum, M. Hoferichter, H. Krebs, B. Kubis, and U. G. Meissner, Physics Letters B **770**, 27 (2017).

[28] S. Wesolowski, I. Svensson, A. Ekström, C. Forssén, R. J. Furnstahl, J. A. Melendez, and D. R. Phillips, Phys. Rev. C **104**, 064001 (2021).

[29] R. N. Pérez, J. E. Amaro, and E. R. Arriola, Phys. Rev. C **88**, 064002 (2013).

[30] R. N. Pérez, J. E. Amaro, and E. R. Arriola, Phys. Rev. C **91**, 054002 (2015).

[31] R. N. Pérez, J. E. Amaro, and E. Ruiz Arriola, Phys. Rev. C **95**, 064001 (2017).

[32] R. Machleidt and D. R. Entem, Phys. Rept. **503**, 1 (2011), arXiv:1105.2919 [nucl-th].

[33] Note that NLO in the pion-nucleon sector corresponds to NNLO in the NN interaction.

[34] E. Epelbaum, A. Gasparyan, J. Gegelia, and H. Krebs, Nuclear Forces for Precision Nuclear Physics–a collection of perspectives– , 47 (2022).

[35] R. J. Hill, P. Kammel, W. J. Marciano, and A. Sirlin, Rept. Prog. Phys. **81**, 096301 (2018), arXiv:1708.08462 [hep-ph].

[36] R. J. Furnstahl, N. Klco, D. R. Phillips, and S. Wesolowski, Phys. Rev. C **92**, 024005 (2015).

[37] M. Gorchtein, Phys. Rev. Lett. **123**, 042503 (2019), arXiv:1812.04229 [nucl-th].

[38] R. L. Workman and Others (Particle Data Group), PTEP **2022**, 083C01 (2022).

[39] G. Shen, L. E. Marcucci, J. Carlson, S. Gandolfi, and R. Schiavilla, Phys. Rev. C **86**, 035503 (2012).